Modelling of an exhaust air heat pump used for heating and domestic hot water production

Frédéric Ransy[1]*, Samuel Gendebien[1], Vincent lemort[1]

(1) Thermodynamics Laboratory, University of Liege, Liège, Belgium

1. ABSTRACT

Exhaust heat pump is a promising solution to heat and ventilate a building with a high energy efficiency, and a competitive investment cost. The authors presented in 2015 laboratory test results about an exhaust heat pump and showed a COP of 4.4 for the conditions A22W35. A simple annual extrapolation of the results showed a similar primary energy consumption than the conventional balanced ventilation system combined with an outside air heat pump. However, the authors presented in 2018 the performance of the same machine integrated in a demonstration building in Belgium. Due to the ultra-low heating capacity (1500 W), the measured overall COP of the system was 2.18. In order to increase the heating capacity of the system, this paper presents a semi-empirical model of the heat pump to study the impact of the design of the different elements of the machine on the performance.

Keywords: Exhaust air heat pump, modelling, experimental

2. INTRODUCTION AND CONTEXT

In Belgium, typical HVAC systems installed in highly efficient residential buildings consist of a centralized balanced ventilation with heat recovery, combined with a gas condensing boiler or a heat pump for space heating and domestic hot water production. In this combination of systems, the ventilation and the heating systems are decoupled, and are therefore easy to control. However, the balanced ventilation system with heat recovery is characterized by a high electrical consumption, due to the presence of the supply and the exhaust fans and the relatively high specific fan power (Laverge et al., 2012). Moreover, the condensing boiler technology is a fossil-fuel based technology and emits CO_2. The heat pump is a good environmental-friendly alternative. On the other hand, the heat pump technology remains expensive and the investment is sometimes hardly justifiable in residential construction projects because the building energy demand is very low.

The performance of typical HVAC systems can be improved through two different aspects: the ventilation and the heating system.

For example, Gendebien et al. presented in 2013 a single room ventilation device with heat recovery, characterized by a lower specific fan power than conventional centralized units. However, by definition, one decentralized unit must be installed in each room where a ventilation airflow is necessary. It can lead to a high investment cost in residential construction projects. The noise level in bedrooms during the nights can also be a problem. Recently, the concept of smart ventilation strategies was also introduced in the literature (Guyotab et al, 2017). The concept is to control the ventilation airflows based on the CO_2 and the humidity levels. Consequently, the fan electrical consumption is lower, and the overall energy consumption of the ventilation can be decreased by 50%. However, the use of sensors increases the complexity and the investment cost of the system.

Concerning the heating system, many researchers are currently developing technologies to increase the performance of actual heat pump systems, such as heat pumps with vapor injection (Dechesne et al, 2017), the development of new fluids (Nawaz et al., 2017 and Zhang et al., 2015) or advanced multivariable fuzzy logic control (Underwood, 2015). In addition, other renewable energy technologies are currently available on the market: micro-CHP, biomass boiler, … The major disadvantage of these systems is the investment cost which is prohibitive for residential projects without government support.

This paper presents another technology used to ventilate and heat highly efficient residential buildings: the exhaust air heat pump. Figure 1 shows a typical integration of an exhaust air heat pump in a residential building.

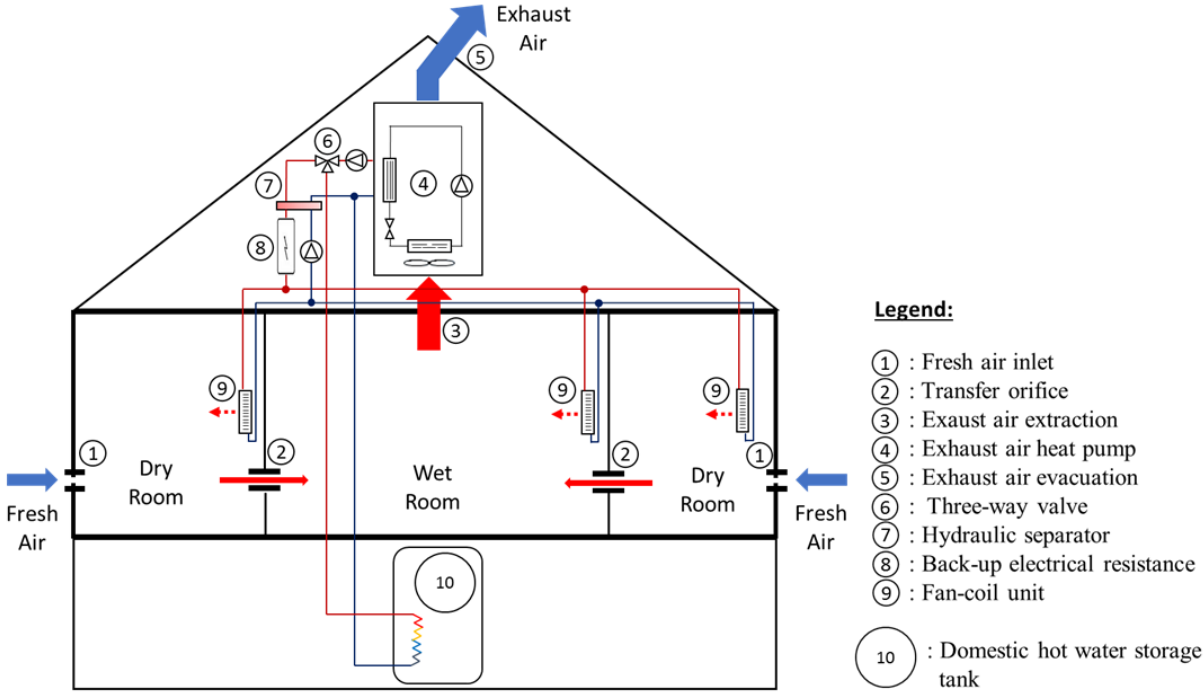

Figure 1: Typical integration of an exhaust air heat pump in residential buildings

In this system, the evaporator of the heat pump is located in the exhaust air flow of the mechanical exhaust ventilation system and the condenser is connected to the heating circuit of the house. The heat pump also provides the heat required for the hot water production, stored in a storage tank. The system can be coupled with fan-coil units or floor heating. If the heat pump cannot cover the whole building energy demand, an electrical resistance is activated.

The air temperature at the supply of the exhaust air heat pump is relatively constant over the year, i.e. between 18 and 23°C. By comparison, the cold source temperature of a conventional outside air heat pump varies from -10 to 15°C during winter. Consequently, the seasonal COP of an exhaust air heat pump is theoretically higher than conventional heat pump (Fracastoro et al., 2010). Moreover, the heating capacity, the COP and the operating conditions are constant over the year. For this reason, exhaust air heat pump can be cost-effective by keeping the design of the machine as simple as possible.

In the proposed building integration scheme (Figure 1), the exhaust air heat pump is combined with an exhaust ventilation system. Compared to the balanced (supply + exhaust) mechanical ventilation system, the fan electrical consumption is lower, because only one fan is required. The whole system performs a combination of three functions: ventilation, heating and domestic

hot water production. For this reason, from an economic point of view, the system is a competitive alternative to conventional HVAC systems.

However, the system has two main disadvantages. Firstly, the heating demand of the building is much higher in the case of an exhaust mechanical ventilation, compared to a balanced ventilation system with heat recovery. Secondly, the heating capacity of the exhaust air heat pump is limited by the maximum ventilation airflow of the house. Consequently, if the heating capacity is not sufficient, the backup resistance is activated, and the COP of the whole system decreases.

In order to quantify the real performance of an exhaust air heat pump integrated in a typical residential building, several models of exhaust air heat pumps were tested experimentally in the thermodynamics laboratory of the University of Liege in Belgium. The results were presented for one machine in 2015 by the authors. The COP of the system for the conditions A22W35 (air supply temperature of 22°C and water exhaust temperature of 35°C) was equal to 4.4. A numerical model of the exhaust air heat pump was developed, and integrated into a numerical model of an apartment, representative of the Belgian building stock. The building model was presented in 2016 by the authors. The annual simulations of the system showed that the exhaust air heat pump and the balanced ventilation system coupled to an outside air heat pump were similar in terms of primary energy consumption.

To confirm these good results, an exhaust air heat pump was installed in 2016 in a demonstration building in Belgium. The heating capacity of the heat pump was 1500 Watts in nominal conditions (A20W35). The building was a new single-family freestanding house with two stories. The results were presented in 2018 by the authors.

The results showed good performance of the exhaust air heat pump. Indeed, in space heating mode with an average exhaust water temperature of 45°C, the average COP of the machine was equal to 3.55. In domestic hot water production mode, the average COP was equal to 3.44, with a domestic hot water set-point temperature of 50°C.

However, due to the limited heating capacity of 1500 W, the exhaust air heat pump was not able to provide the whole energy demand of the building, particularly in winter. Consequently, the electrical backup resistance was activated and the whole system efficiency decreases. A simple annual extrapolation of the results showed an annual coverage factor of 76 % and a seasonal COP of 2.18. This value is significantly lower than the theoretical value of 3.4 that could be achieved if the heat pump could cover the whole building energy demand.

In conclusion, the main problem of exhaust air heat pumps is the limited heating capacity, due to the limited ventilation airflow. The objective of this paper is to show what could be the maximum heating capacity of an exhaust air heat pump, if the ventilation airflow is fixed at a typical value for freestanding residential buildings. A second objective is also to show the impact on the design of the machine, and on the risk of frost formation on the evaporator.

For this purpose, a semi-empirical model of the heat pump is presented. For each component of the machine, the geometry is considered, in order to evaluate the impact of the design on the heating capacity and the performance. The model of each component is calibrated with experimental data from laboratory tests and the heat pump model is validated with five data set.

3. HEAT PUMP MODELLING

This section presents the semi-empirical model of the exhaust air heat pump developed in Matlab. In this type of model, the parameters have a physical meaning. The model can then be used to extrapolate the performance of the machine for non-tested conditions. The three main components of the system are the compressor, the condenser and the evaporator.

3.1 Compressor

The compressor is an air cooled and hermetic rolling piston compressor working with R134a. Rotary compressors are popular in low capacity air conditioning and refrigeration systems. Its control is a simple ON/OFF switch.

The semi-empirical model was initially developed for scroll, reciprocating, and screw compressors (Dardenne et al, 2015, Giuffrida, 2016, Li, 2013, Winandy et al, 2002, Lemort et al, 2009). The compression process from the suction to the discharge is described through elementary thermodynamic transformations that represent the thermodynamic processes accomplished by the refrigerant inside the compressor. The model considers the losses due to the internal heat exchanges, the heat losses to the environment, the internal leakage, the exhaust pressure drop and the electro-mechanical losses. A schematic representation of the compressor model is presented in Figure 2.

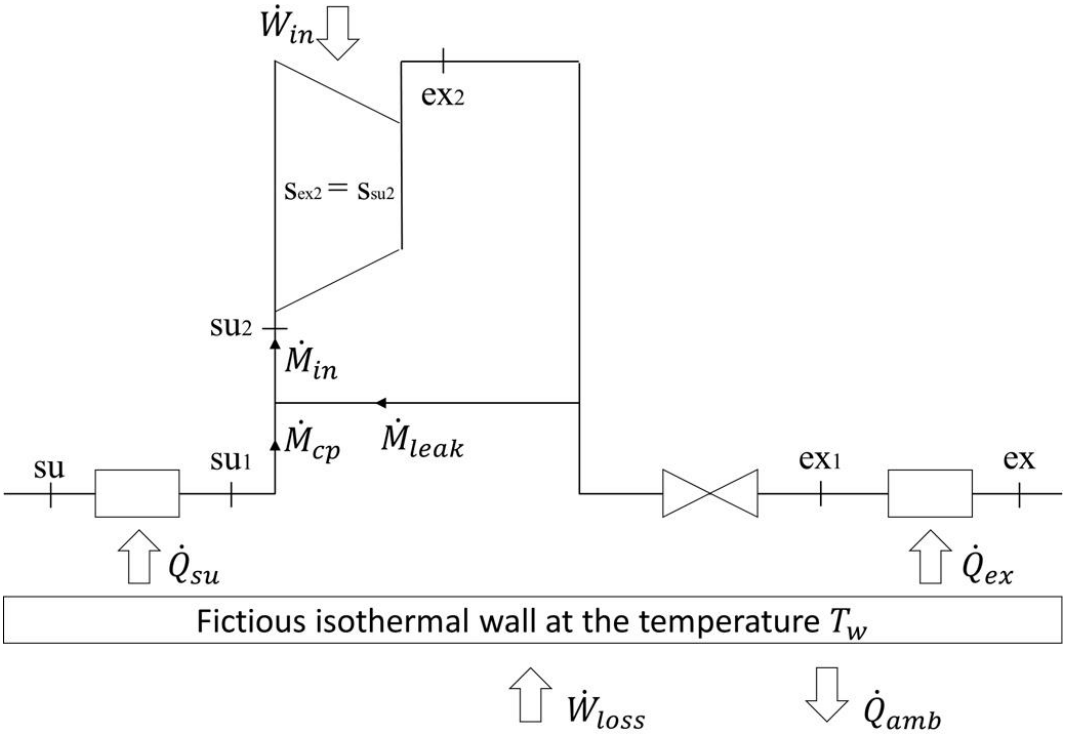

Figure 2: Schematic representation of the compressor model

In the model, the refrigerant is supposed to undergo the following transformations:

- su – su1: isobaric ($P_{su1} = P_{su}$) heating-up of the supply refrigerant mass flow rate,
- su1 – su2: isobaric ($P_{su2} = P_{su1}$) mixing of the supply mass flow with the internal leakage,
- su2 – ex2: isentropic ($s_{ex2} = s_{su2}$) compression,
- ex2 – ex1: isenthalpic ($h_{ex1} = h_{ex2}$) exhaust pressure drop through the discharge valve,
- ex1 – ex: isobaric ($P_{ex} = P_{ex1}$) cooling-down of the exhaust refrigerant mass flow rate.

The following sections describe the equations relative to the above-mentioned thermodynamic transformations.

Supply isobaric heat transfer

Internal heat transfers occur between the fluid, the compressor, the motor and the oil. In the present model, the internal heat transfers lead to a heating at the supply and a cooling at the exhaust. To compute the heat transfers, a fictious isothermal wall at the temperature T_w is

introduced. This isothermal wall exchanges thermal energy with the refrigerant, the motor (through the electro-mechanical losses, described in the following) and the ambient.
For the modelling of the heat exchange at the supply, a semi-isothermal heat exchanger is considered, and the ε-NTU method is used to determine the exchanger efficiency. The equations describing the heat transfer at the supply are the following:

$$\dot{Q}_{su} = \dot{M}_{cp}(h_{su1} - h_{su}) = \varepsilon_{su}\, \dot{M}_{cp} c_{p,su}(T_w - T_{su}) \quad (1)$$

$$\varepsilon_{su} = \left(1 - e^{\left(\frac{-AU_{su}}{\dot{M}_{cp}\, c_{p,su}}\right)}\right) \quad (2)$$

$$AU_{su} = AU_{su,n} \left(\frac{\dot{M}_{cp}}{\dot{M}_{cp,n}}\right)^{0.8} \quad (3)$$

The two parameters are the nominal overall heat transfer coefficient at the supply, $AU_{su,n}$, and the corresponding nominal mass flow rate, $\dot{M}_{cp,n}$.

Internal leakage and isobaric mixing with supply mass flow rate

In rolling piston compressors, due to clearance between the wall of the rolling piston and the cylinder, leakages occur from the compression to the suction chambers. In the model, the enthalpy of the leakage mass flow rate is supposed to be the enthalpy at the exhaust of the isentropic compression, h_{ex2}. The leakage mass flow rate is then mixed with the supply refrigerant mass flow rate, before the isentropic compression. The following equations are used for the mixing:

$$\dot{M}_{in} = \dot{M}_{cp} + \dot{M}_{leak} \quad (4)$$

$$\dot{M}_{in}\, h_{su2} = \dot{M}_{cp}\, h_{su1} + \dot{M}_{leak}\; h_{ex2} \quad (5)$$

An isentropic flow through a simply convergent nozzle is considered to calculate the leakage mass flow rate:

$$\dot{M}_{leak} = A_{leak}\, \rho(s_{ex2}, P_{thr}) \sqrt{2[h_{ex2} - h(s_{ex2}, P_{thr})]} \quad (6)$$

The nozzle throat A_{leak} is a parameter of the model to be identified. In Eq. 6, the throat pressure P_{thr} is the maximum between the throat outlet pressure and the critical low pressure corresponding to choked flow conditions, considering the refrigerant vapor as a perfect gas:

$$P_{thr} = \max\left(P_{su1}, P_{ex2} \left(\frac{2}{\gamma_{ex2} + 1}\right)^{\frac{\gamma_{ex2}}{\gamma_{ex2}-1}}\right) \quad (7)$$

The internal mass flow rate $\dot{M}_{in}$ depends on the swept volume of the compressor, V_s, the rotational speed of the compressor, N, and on the density of the refrigerant after the mixing process:

$$\dot{M}_{in} = \rho_{su2}\, V_s\, \frac{N}{60} \quad (8)$$

The compressor swept volume V_s is parameter to be identified and is generally given by the manufacturer. In the following sections, the value given by the manufacturer is supposed to be the good value. For a ON-OFF compressor, the rotational speed N is constant and generally equal to 3000 rpm.

Isentropic compression and isenthalpic exhaust pressure drop

In the model, the compression from the suction su2 to the exhaust ex2 is supposed to be isentropic. To determine the thermodynamic state at the end of the isentropic compression, the internal discharge pressure P_{ex2} needs to be determined. This pressure depends on the pressure drop at the exhaust of the compressor. Indeed, rolling piston compressors are manufactured with a discharge valve. Consequently, the internal discharge pressure is always higher than the actual exhaust pressure, to ensure a complete exhaust-gas discharge from the combustion chamber to the exhaust port. In the model, the exhaust refrigerant flow through the discharge valve is considered in the same way as for the leakage, i.e. an isentropic flow through a simply convergent nozzle. The same equations apply:

$$\dot{M}_{cp} = A_{dis}\,\rho\left(s_{ex2}, P_{thr,dis}\right)\sqrt{2[h_{ex2} - h\left(s_{ex2}, P_{thr,dis}\right)]} \tag{9}$$

$$P_{thr,dis} = \max\left(P_{ex}, P_{ex2}\left(\frac{2}{\gamma_{ex2}+1}\right)^{\frac{\gamma_{ex2}}{\gamma_{ex2}-1}}\right) \tag{10}$$

The parameter A_{dis} is the area of the discharge valve and is a parameter to be identified.

Exhaust isobaric heat transfer

The modelling approaches for the exhaust and the supply heat transfers are the same. Consequently, the equations are similar:

$$\dot{Q}_{ex} = \dot{M}_{cp}(h_{ex} - h_{ex1}) = \varepsilon_{ex}\,\dot{M}_{cp} c_{p,ex1}(T_w - T_{ex1}) \tag{11}$$

$$\varepsilon_{ex} = \left(1 - e^{\left(\frac{-AU_{ex}}{\dot{M}_{cp}\,c_{p,ex1}}\right)}\right) \tag{12}$$

$$AU_{ex} = AU_{ex,n}\left(\frac{\dot{M}_{cp}}{\dot{M}_{cp,n}}\right)^{0.8} \tag{13}$$

The two parameters are the nominal overall heat transfer coefficient at the exhaust, $AU_{ex,n}$, and the corresponding nominal mass flow rate, $\dot{M}_{cp,n}$.

Electrical consumption

The compressor electrical power input is the sum of the compressor internal power and the electro-mechanical losses. The electro-mechanical losses are split into two terms: constant losses and losses proportional to the internal power:

$$\dot{W}_{cp} = \dot{W}_{in} + \dot{W}_{loss} = \dot{M}_{in}\,(h_{ex2} - h_{su2}) + \dot{W}_{loss} \tag{14}$$

$$\dot{W}_{loss} = 2\,\pi\,N\,T_{loss} + \alpha\,\dot{W}_{in} \tag{15}$$

The two parameters to be identified are the constant mechanical loss torque T_{loss} and the factor of proportionality α for the electro-mechanical loss proportional to the internal power. The electro-mechanical losses are directly injected into the fictious envelope.

Fictitious envelope heat balance and heat losses to the environment

To close the system of equations, the heat balance applied on the fictious envelope on steady-state is written:

$$\dot{W}_{loss} - \dot{Q}_{ex} - \dot{Q}_{su} - \dot{Q}_{amb} = 0 \quad (16)$$

The last term in Eq. 16 is the heat losses to the environment. Different formulations exist in the literature to calculate the compressor ambient heat losses. For example, a simple constant overall heat transfer coefficient to the ambient can be used. In the case proposed in this paper, this modeling method is not sufficiently accurate. Indeed, the compressor is cooled down by the ventilation airflow. As a result, due to the important airflow around the compressor, the ambient heat losses can represent a non-negligible fraction of the compressor consumption (from 10 to 40%). The compressor performance can thus be largely influenced by the ventilation airflow. A mode detail model of ambient heat losses is consequently proposed in the following.

The Figure 3 represents a 2-D top view of the relative positions the compressor and the evaporator in the heat pump casing. The airflow enters the heat pump and directly cools down the compressor. The heated air is then sent to the evaporator, is cooled down, and exits the heat pump. The air temperature at the supply of the evaporator directly depends on the convective heat losses. This temperature will influence the evaporator heat exchange, and the overall performance of the machine.

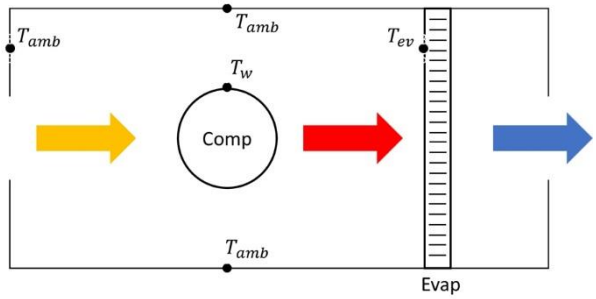

Figure 3: 2-D representation of the position of the compressor, the evaporator and the heat pump casing

The compressor heat losses $\dot{Q}_{amb}$ are divided in two terms: the radiative heat exchange with the surrounding surfaces, $\dot{Q}_{amb,r}$, and the convective heat transfer with the supply air, $\dot{Q}_{amb,c}$.

For the radiative heat exchange, the compressor is supposed to exchange energy with the casing of the heat pump, and with the surface of the evaporator, which is situated close to the compressor. The surface temperature of the casing is supposed to be the ambient temperature, T_{amb} , and the surface temperature of the evaporator is supposed to the evaporating temperature, T_{ev}. For the convective heat exchange, the heat flow depends on the convective heat transfer coefficient. The equations are the following:

$$\dot{Q}_{amb} = \dot{Q}_{amb,c} + \dot{Q}_{amb,r} \quad (17)$$

$$\dot{Q}_{amb,r} = \sigma\, \varepsilon_{cp}\, A_{ext,cp} \left(\left(F_{cp,ev} (T_w^4 - T_{ev}^4) + (1 - F_{cp,ev}) (T_w^4 - T_{amb}^4) \right) \right) \quad (18)$$

$$\dot{Q}_{amb,c} = A_{ext,cp}\, h_{c,cp} \left(T_w - T_{a,su} \right) \quad (19)$$

with σ the Stefan–Boltzmann constant, ε_{cp} the emissivity of the compressor casing, assumed to be 0.95, $A_{ext,cp}$ the outer surface of the compressor $\left(= \pi \frac{D_{ext,cp}^2}{4} + \pi\, D_{ext,cp} H_{cp} \right)$, $F_{cp,ev}$ the view factor from the compressor to the evaporator, T_w the surface temperature of the

compressor casing, $T_{a,su}$ the air supply temperature and $h_{c,cp}$ the convective heat transfer coefficient. The following correlation is used to determine the heat transfer coefficient:

$$h_{c,cp} = \frac{Nu.k}{D_{ext,cp}} \tag{20}$$

$$Nu = C_{Nu} Re_{D_{ext,cp}}^{n_{Nu}} Pr^{1/3} \tag{21}$$

$$Re_{D_{ext,cp}} = \frac{V_{su} D_{ext,cp}\, \rho}{\mu} \tag{22}$$

The two constants C_{Nu} and $n_{Nu}$are two empirical parameters of the model to be identified.

Variation of the semi-empirical parameters with the compressor size

The semi-empirical parameters described in the previous sections are identified for one compressor size, i.e. one value of the swept volume V_s. However, the objective of the heat pump model is to predict the variation of the performance if the geometries of the constituting elements are changed. If the parameters are known for one compressor swept volume $V_{s,n}$, the parameters corresponding to another swept volume $V_{s,2}$ are calculated as followed:

$$AU_{su,n,\,V_s=V_s} = AU_{su,n,\,V_s=V_{s,n}} \left(\frac{V_s}{V_{s,n}}\right)^{n_1} \tag{23}$$

$$A_{leak,\,V_s=V_s} = A_{leak,\,V_s=V_{s,n}} \left(\frac{V_s}{V_{s,n}}\right)^{n_2} \tag{24}$$

$$A_{dis,\,V_s=V_s} = A_{dis,\,V_s=V_{s,n}} \left(\frac{V_s}{V_{s,n}}\right)^{n_3} \tag{25}$$

$$T_{loss,\,V_s=V_s} = T_{loss,\,V_s=V_{s,n}} \left(\frac{V_s}{V_{s,n}}\right)^{n_4} \tag{26}$$

The four constants n_1, n_2, n_3 and n_4 are identify with at least two set of experimental data from two compressors with a different swept volume. The two compressor technologies must be the same.

3.2 Condenser

The condenser consists of a brazed plate heat exchanger. The working fluid is the refrigerant R134a and the secondary fluid is liquid water. The principal geometric characteristics of the condenser are listed in Table 1.

L_{hex} $[m]$	W_{hex} $[m]$	p $[m]$	φ [°]	Φ [-]	th_p [mm]	N_p [-]
0.247	0.191	0.00152	30	1.22	0.4	24

Table 1: Geometric characteristics of the condenser

In the model, the condenser is divided in three zones: the superheated vapor, the two-phase flow and the subcooled liquid. The modelling principle is represented in Figure 4. The model supposes a counterflow heat exchange.

For each zone i, the two heat balances in steady state on the water side and on the refrigerant side are expressed as:

$$\dot{Q}_{cd,i} = \dot{M}_r \, (h_{r,su,i} - h_{r,ex,i}) \tag{27}$$

$$\dot{Q}_{cd,i} = \dot{M}_w \, cp_w \, (T_{w,ex,i} - T_{w,su,i}) \tag{28}$$

with $i = v, tp \; or \; l$.

To calculate the heat flow in each zone, the logarithmic mean temperature difference is calculated as followed:

$$\dot{Q}_{cd,i} = A_i \, U_i \, \Delta T_{log,i} \tag{29}$$

with A_i the heat transfer area of each zone, $\Delta T_{log,i}$ the logarithmic mean temperature difference between the working fluid and the secondary in each zone and U_i the overall heat transfer coefficient for each zone. This coefficient depends on the convective heat transfer coefficient on the water side, on the convective heat transfer coefficient on the refrigerant side and on the conductive thermal resistance of the plates. It is calculated as followed:

$$U_i = \frac{1}{\frac{1}{h_{i,sf}} + \frac{th_p}{k_p} + \frac{1}{h_{i,wf}}} \tag{30}$$

The heat transfer coefficient for the secondary fluid (water) and for the working fluid (refrigerant) in the superheated zone and the subcooled zone are calculated with the correlation proposed by Martin (1996). In this approach, the heat transfer coefficient depends only on geometrical characteristics of the exchanger. The heat transfer on the working fluid in the two-phase flow is determined with the correlation proposed by Longo (2015).

The total condenser heat flow rate is the sum of the heat flows in each zone:

$$\dot{Q}_{cd} = \dot{Q}_{cd,v} + \dot{Q}_{cd,tp} + \dot{Q}_{cd,l} \tag{31}$$

In the proposed model, it is not necessary to tune empirical parameters because all the calculations are based only on the geometrical characteristics of the exchanger.

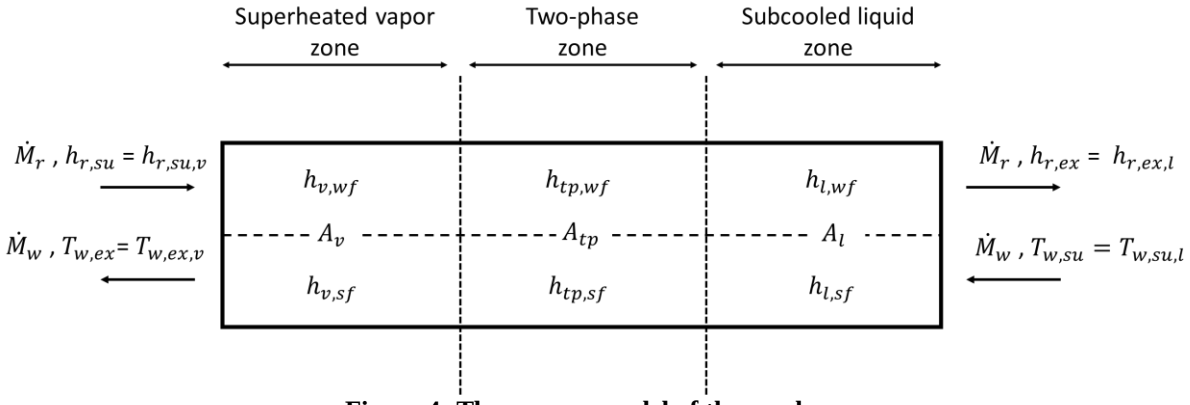

Figure 4: Three zones model of the condenser

3.3 Evaporator

The evaporator consists of a finned-tube heat exchanger. The working fluid is the refrigerant R134a and the secondary fluid is the air. The principal geometric characteristics of the condenser are listed in Table 2.

The modeling of the evaporator consists in assuming that the heat exchanger is semi-isothermal, with the constant temperature equal to the saturation temperature. It is assumed that the

exchanger works in a completely dry regime, or a completely wet regime. The exchanger thermal output is the maximum of the heat exchange in the two regimes:

$$\dot{Q}_{ev} = \max(\dot{Q}_{ev,dry}, \dot{Q}_{ev,wet}) \quad (32)$$

The heat exchange in dry regime is calculated with the $\varepsilon - NTU$ method:

$$\dot{Q}_{ev,dry} = \varepsilon_{dry} \dot{M}_a cp_a (T_{a,su} - T_{ev,dry}) \quad (33)$$

The efficiency in dry regime depends on the overall heat transfer coefficient:

$$\varepsilon_{dry} = 1 - \exp\left(\frac{-AU_{dry}}{\dot{M}_a cp_a}\right) \quad (34)$$

The overall heat transfer coefficient depends on the wall thermal resistance, the total air heat transfer area, the fin efficiency, the air side convective heat transfer coefficient, the refrigerant convective heat transfer coefficient and the inside heat transfer area on the refrigerant side:

$$AU_{dry} = \frac{1}{\frac{1}{A_{a,tot}\,\eta_{f,dry} h_{a,dry}} + R_{cu} + \frac{1}{A_{r,in} h_{r,boiling}}} \quad (35)$$

The total air transfer area, the fin efficiency and the inside heat transfer area depends only on the geometrical characteristics of the evaporator. The air side convective heat transfer coefficient is determined with the correlation proposed by Wang et al. (2000). The refrigerant convective heat transfer coefficient inside the tube is determined with the Shah (1982) correlation.

To calculate the exhaust air temperature and the enthalpy of the refrigerant at the exhaust, the two heat balances apply:

$$\dot{Q}_{ev,dry} = \dot{M}_r (h_{r,ex,dry} - h_{r,su,ev}) \quad (36)$$

$$\dot{Q}_{ev,dry} = \dot{M}_a cp_a (T_{a,su} - T_{a,ex,dry}) \quad (37)$$

In wet regime, the moist air is replaced by a fictitious ideal gas with a specific heat cp_f given by:

$$cp_f = \frac{h_{a,su} - h_{a,ex}}{T_{wb,su} - T_{wb,ex}} \quad (38)$$

The equations 33, 34, 35, 36 still apply to calculate the heat exchange in wet regime, but with $cp_a = cp_f$ and $T_{a,su} = T_{wb,su}$. Moreover, the air side convective heat transfer coefficient is corrected as followed:

$$h_{a,wet} = h_{a,dry} \frac{cp_f}{cp_a} \quad (39)$$

It should be also noticed that the fin efficiency η_f is lower in wet regime than in dry regime.

To determine the exhaust air humidity ratio, the hypotheses proposed by ASHRAE (2000) are used.

$N_T[-]$	$N_L[-]$	$L[m]$	W[m]	H[m]	δ_f[mm]	P_L[m]	P_T[m]	F_p [m]
10	3	0.065	0.3	0.24	0.115	0.02	0.025	0.0025

Table 2: Geometric characteristics of the evaporator

3.4 Heat pump

The heat pump model associates the sub-models of the rolling piston compressor, the evaporator and the condenser. The information flow diagram is presented in Figure 5.

For given supply conditions and exhaust pressure, the compressor model imposes the refrigerant mass flow rate. The compressor rotational speed is fixed at 3000 rpm. The compressor heat losses are calculated based on the supply airflow and temperature.

For a given water mass flow rate, refrigerant mass flow rate, supply refrigerant temperature and supply water temperature, the condenser model imposes the condensing pressure. The liquid subcooling at the condenser exhaust is imposed at 5K.

The expansion valve model assumes that expansion is isenthalpic, which imposes the vapor enthalpy at the evaporator supply. It also imposes the vapor superheat at evaporator exhaust, fixed at 5K.

For a given supply refrigerant mass flow rate, given supply temperature and air humidity and a given air mass flow, the evaporator imposes the evaporating pressure. The air supply temperature depends on the compressor heat losses and air mass flow.

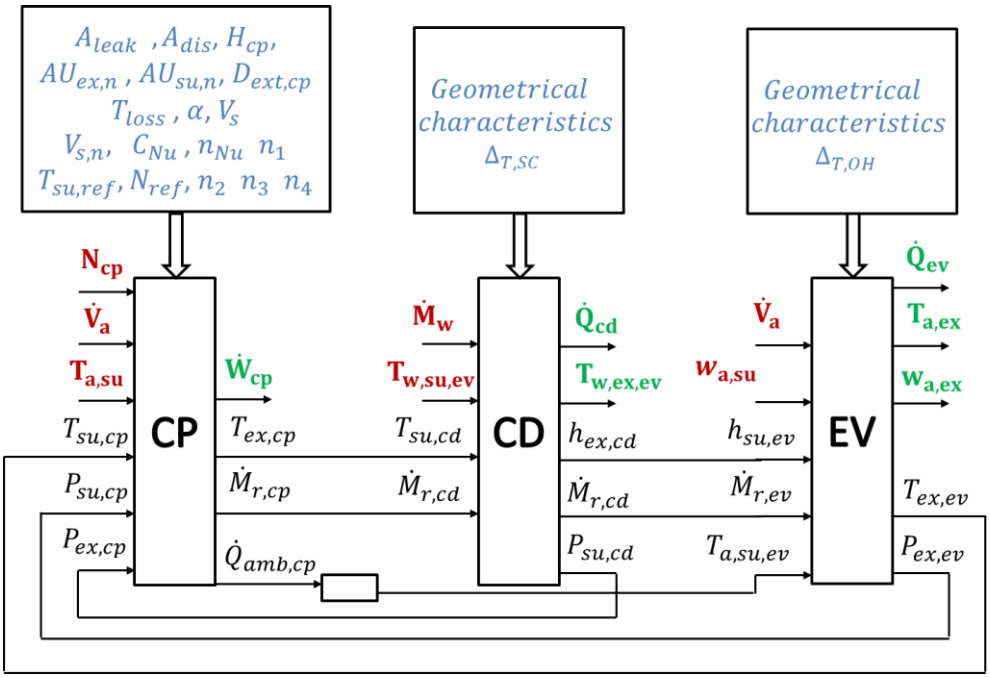

Figure 5: Schematic representation of the heat pump model

4. PARAMETERS IDENTIFICATION

This section describes the methodology used to identify the parameters of the compressor, the condenser and the evaporator. The predicted values with the model are compared with the experimental values obtained in laboratory conditions.

4.1 Methodology

The compressor model has 18 parameters. The three parameters $V_{s,n}$, $T_{su,ref}$ and N_{ref} are reference variables fixed at constant value, respectively 16.12 cm³, 5°C and 3000 rpm. The three parameters H_{cp}, $D_{ext,cp}$ and V_s are geometrical characteristics and do not have to be identified. The remaining parameters are A_{leak}, A_{dis} , $AU_{ex,n}$, $AU_{su,n}$, T_{loss}, α, C_{Nu} and n_{Nu}. These empirical parameters are valid for a fixed compressor swept volume $V_{s,n}$ and are

identified with a set of experimental data obtained during laboratory tests. The last four parameters to be identified are the exponents n_1, n_2, n_3 and n_4. These parameters allow to extrapolate the performance for a different compressor swept volume using the same set of parameters.

The fmincon function of MATLAB is used to minimize the error between the measurement (mea index) and the prediction of the model (mod index). The error function is defined as:

$$E = \sqrt{\frac{\sum_{i=1}^{n}\left(\left(\frac{\dot{W}_{mod-}\dot{W}_{mea}}{\dot{W}_{mod}}\right)^2 + \left(\frac{\dot{M}_{mod-}\dot{M}_{mea}}{\dot{M}_{mod}}\right)^2 + \left(\frac{h_{ex,mod-}h_{ex,mea}}{h_{cex,mod}}\right)^2\right)}{n}} \quad (40)$$

The obtained results are listed in Table 3.

A_{leak} [mm²]	A_{dis} [mm²]	$AU_{ex,n}$ [W/K]	$AU_{su,n}$ [W/K]	T_{loss} [N.m]	α [-]	C_{Nu} [-]	n_{Nu} [-]	n_1 [-]	n_2 [-]	n_3 [-]	n_4 [-]
0.2	113	257	0	0.164	0.41	1.04	0.51	0.43	0	0.57	0.93

Table 3: Parameters of the compressor

The condenser and the evaporator models depend only on geometrical characteristics. Consequently, it is not necessary to identify empirical parameters with experimental data. However, a comparison between experimental and predicted data must be realized to validate the proposed model.

Three heat pumps with different heating capacities were tested over a large range of operating conditions. The condensers and the evaporators of the three machines were the same, for which the geometrical characteristics are given in Table 1 for the condenser and Table 2 for the evaporator. However, the compressor of each heat pump has a different swept volume, equals to 9.52 cm³, 12.75 cm³ and 16.12 cm³. In total, seven tests were performed. During the tests, the heat pumps were connected to a hot water storage tank, allowing the supply water temperature to vary from 15 to 60°C. The Table 4 shows the range of operating conditions for the 7 sets of experimental tests.

Test n°	V_s	$D_{ext,cp}$	H_{cp}	$\dot{M}_w$	$\dot{V}_{air}$	$T_{dp,su}$	$T_{a,su}$	$T_{w,su}$
1 - 1	9.52	0.12	0.22	300	200	9	21	35-55
2 - 1	12.75	0.12	0.23	400	210	10	22	39-57
3 - 1	16.12	0.12	0.24	576	350	10	23	33-57
3 - 2	16.12	0.12	0.24	576	300	10	21	28-55
3 - 3	16.12	0.12	0.24	596	250	10	21	33-57
3 - 4	16.12	0.12	0.24	336	340	9.5	20	21-40
3 - 5	16.12	0.12	0.24	334	350	16-18	22	16-42

Table 4: Range of operating conditions for the 7 sets of experimental tests

In the next sections, the performance predicted by the model are compared with the experimental data, for the compressor, the condenser and the evaporator.

4.2 Compressor

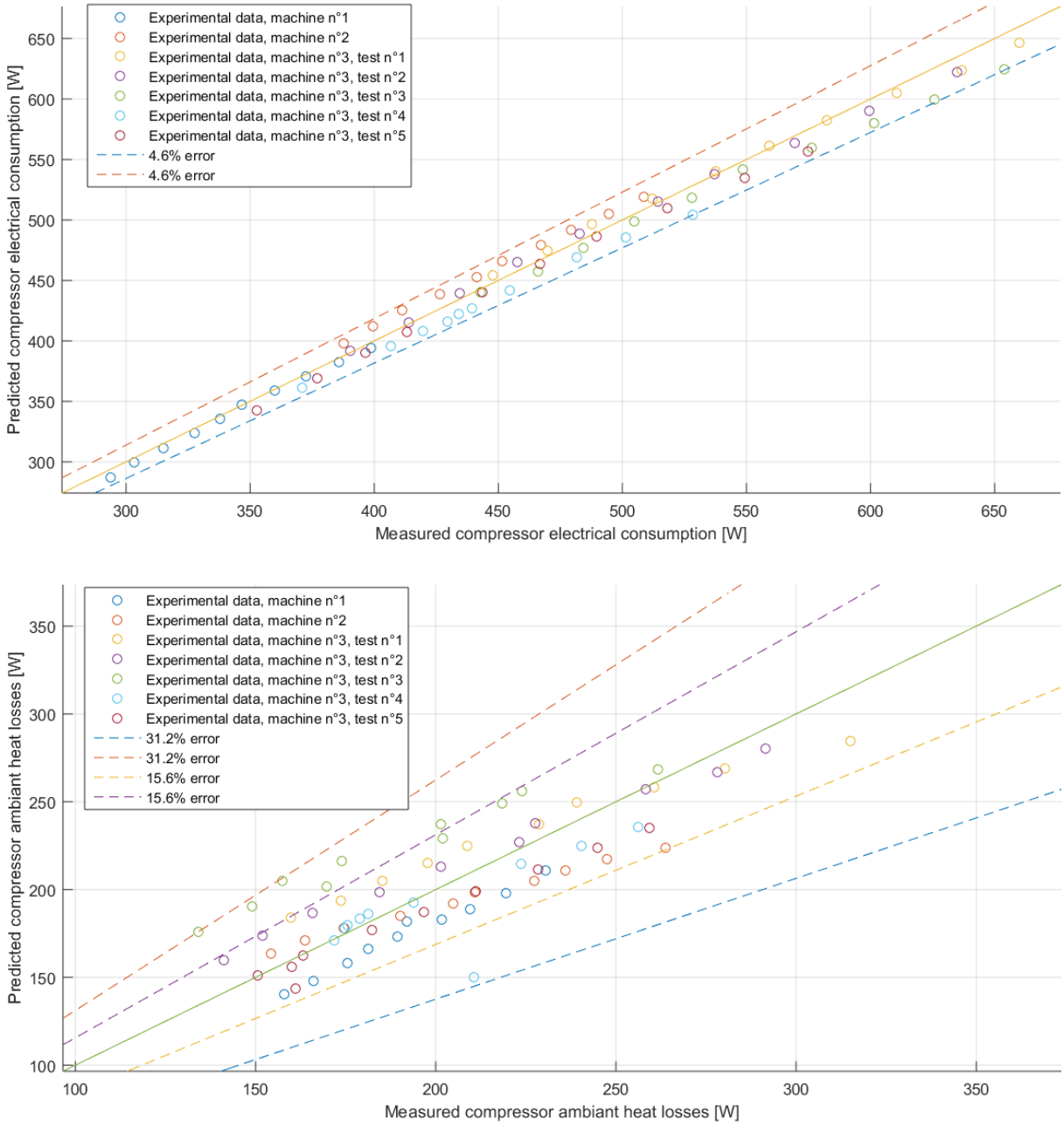

Figure 6: Comparison between simulated and experimental data for the compressor electrical consumption (top) and compressor ambient heat losses (bottom).

This section presents the comparison between simulated and experimental data for the compressor. The Figure 6 shows the comparison for the electrical consumption and the ambient heat losses. For the electrical consumption, the maximum error between the prediction and the experimental data is 5%. The results are very satisfactory considering that three compressors with three different swept volumes are modelled. Concerning the ambient heat losses, the maximum error is 31 % and the error is lower than 15 % for 90 % of the points. These results are considered satisfactory considering the large range of ventilation air values modelled (between 200 and 350 m³/h).

The Figure 7 shows the comparison for the mass flow rate and the exhaust temperature. The maximum error is equal to 5 K. The mas flow rate is predicted with a lower accuracy. Indeed, the maximum error on the mass flow rate is equal to 20%.

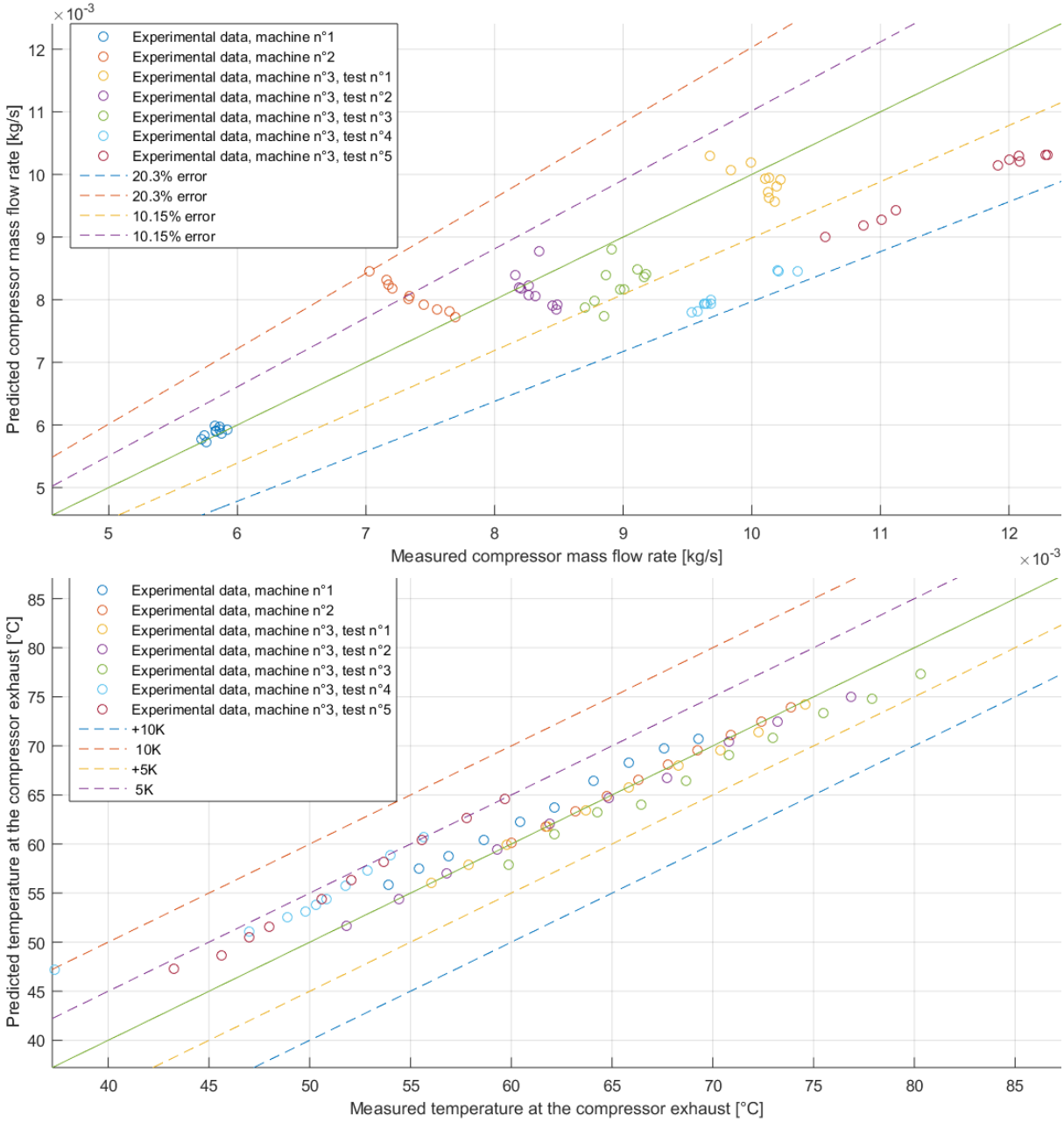

Figure 7: Comparison between simulated and experimental data for the compressor mass flow rate (top) and compressor exhaust temperature (bottom).

4.3 Condenser

This section presents the comparison between simulated and experimental data for the condenser. The Figure 8 shows the comparison for the condensing pressure and the heat flow. The heat flow is very well predicted with a maximum relative error of 4%. The prediction of the model is less accurate for the condensing pressure. In fact, the maximum error on the condensing pressure is 8%. It seems that the model overestimates the condensing pressure, meaning that the overall heat transfer coefficient is under-estimate.

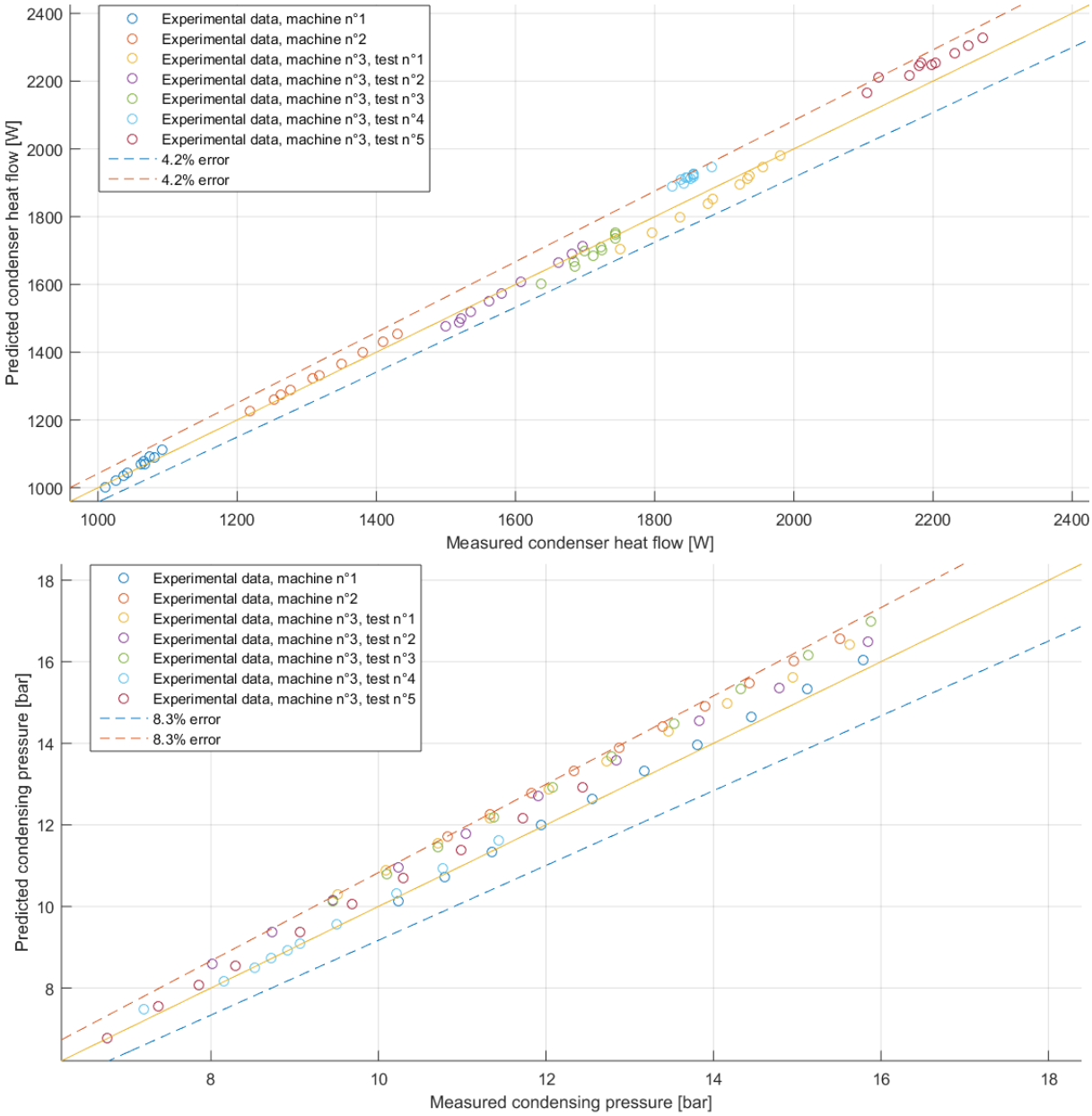

Figure 8: Comparison between simulated and experimental data for the condenser heat flow (top) and the condensing pressure (bottom).

4.4 Evaporator

This section presents the comparison between simulated and experimental data for the evaporator. The results are presented for the tests n°3-4 and n°3-5 because the temperature and the humidity at the exhaust were monitored for these cases only. The Figure 9 shows the comparison for the evaporating pressure and the heat flow. The evaporating pressure is predicted with a good accuracy. The maximum relative error is 7%, and 90 % of the points are predicted with an error lower than 5%. The prediction of the heat flow is even better than the prediction of the evaporating pressure. Indeed, the maximum relative error is lower than 2%. The Figure 10 shows the prediction of the humidity ratio and the dry bulb temperature at the exhaust of the evaporator. Concerning the humidity ratio, the maximum relative error is 15 % and the dry bulb temperature is predicted with an error of 4K.

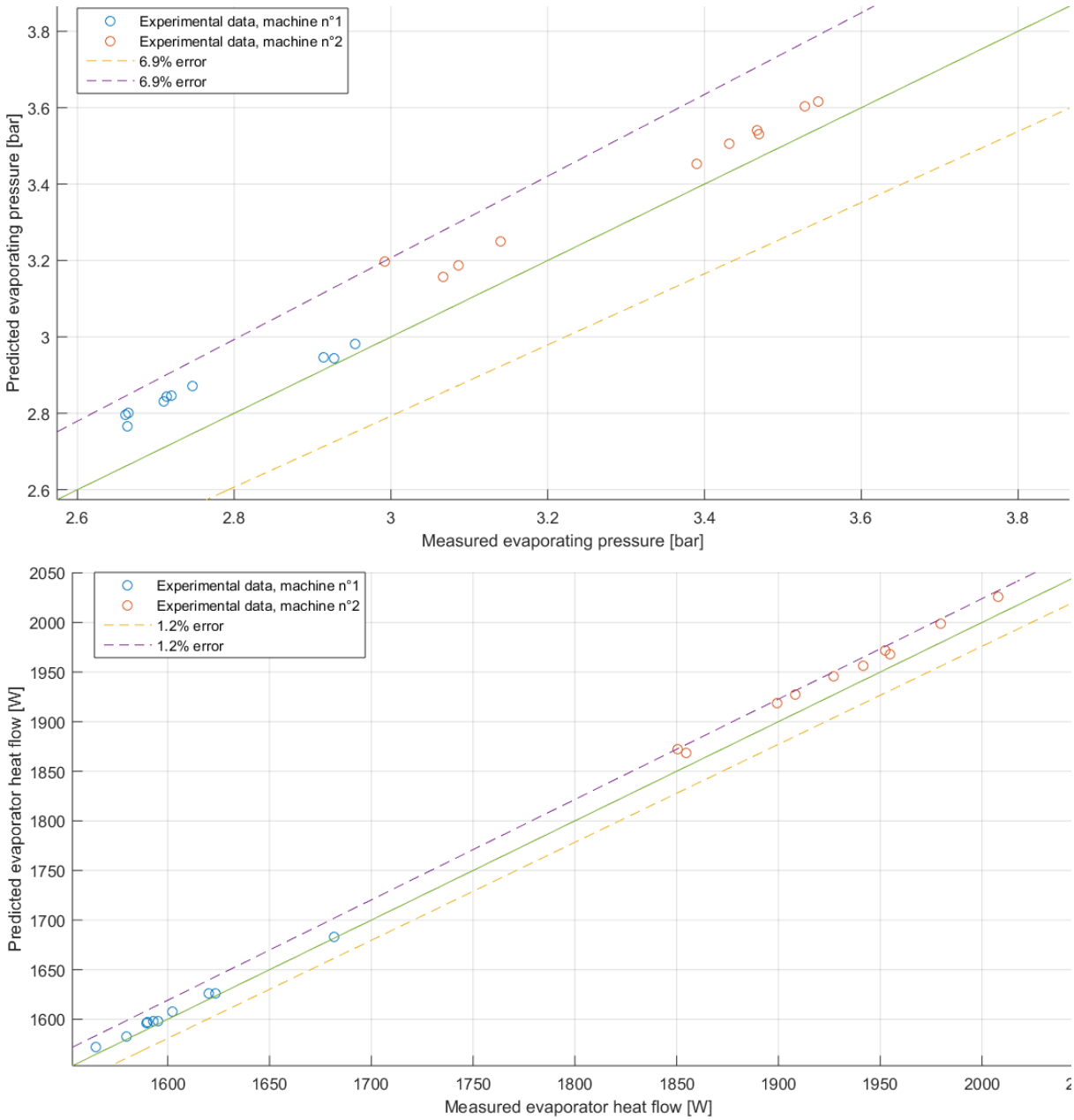

Figure 9: Comparison between simulated and experimental data for the evaporating pressure (top) and the evaporator heat flow (bottom).

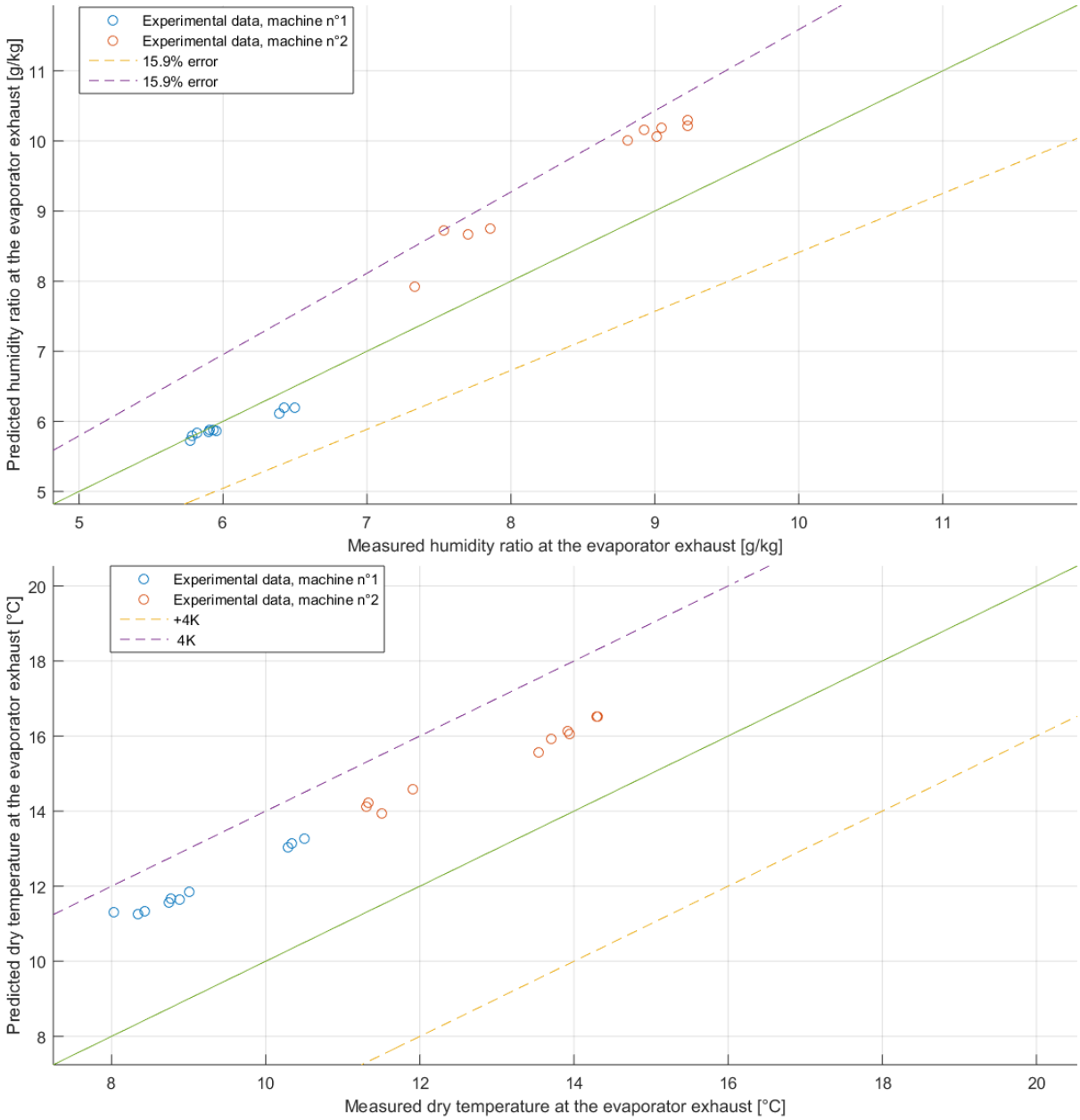

Figure 10: Comparison between simulated and experimental data for the exhaust humidity ratio (top) and the evaporator heat flow (bottom).

5. VALIDATION OF THE HEAT PUMP MODEL

This section presents the validation of the heat pump model and the errors between the predictions and the measurements when all the sub-models are connected. The Figure 11 presents the comparison between simulated and experimental data for the compressor electrical consumption, the condenser heat flow and the COP. The maximum relative error for the compressor electrical consumption is 13%. The consumption seems to be over-estimate for the major part of the point. This is due to the over-estimated value of the condensing pressure. The maximum relative error for the condenser heat flow is 28 %. The predictions relative to the tests n° 1-1, 3-1, 3-3, 3-4 and 3-5 are well predicted, with a relative error lower than 10 %. The data sets n° 2 and 3-2 seems to be problematic and additional research will be undertaken to decrease these errors. The COP is predicted with a relative error of 16%.

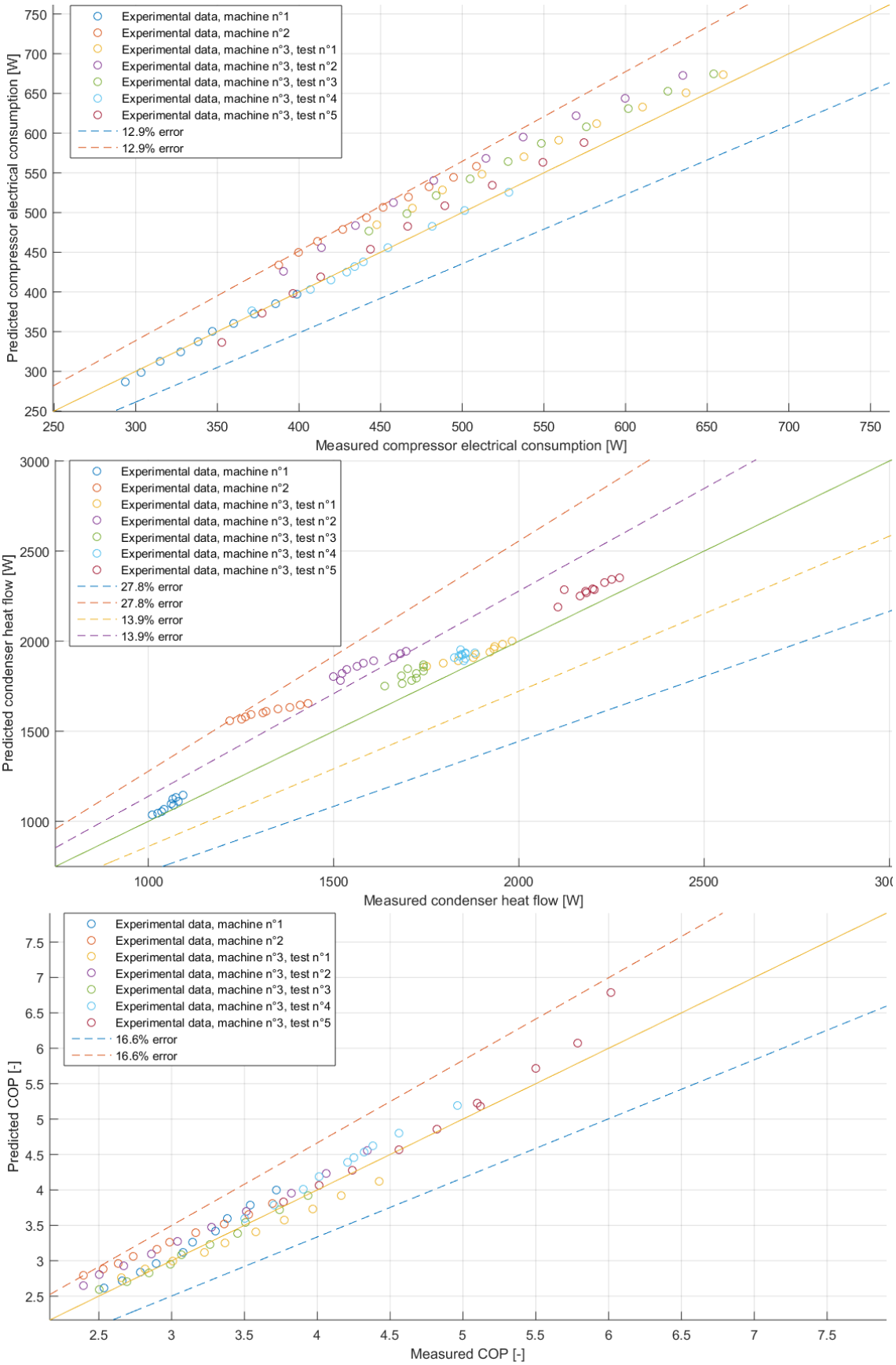

Figure 11: Comparison between simulated and experimental data for the compressor electrical consumption (top), the condenser heat flow (mid) and the COP (bottom).

6. DISCUSSION AND RESULTS

As explained in the introduction, the major drawback of the exhaust air heat pump technology is the limited heating capacity. It can be a problem in freestanding buildings in which a backup resistance is necessary. The objective of this section is to show the heating capacity that could be delivered by an exhaust air heat pump with a bigger compressor (higher compressor swept volume). Ideally, the machine should provide at least 3000 W of heating capacity. The following variables are fixed:

- Volume air flow: 200 m³/h, corresponding to a typical ventilation airflow in freestanding residential buildings,
- Supply air temperature: 20°C,
- Supply dew-point temperature: 10°C,
- Water mass flow rate: 600 l/h.

The Figure 12 shows the variation of the heating capacity of the heat pump with the compressor swept volume. The contact temperature is also represented. With a swept volume of 27 cm³, the heating capacity could reach the value of 2600 W. However, the contact temperature on the evaporator falls below 0°C when the swept volume exceeds 18 cm³. It is problem because frost can appear on the evaporator for a contact temperature lower than 0°C, and this phenomenon decreases the heating capacity and the COP of the machine. Moreover, defrosting strategies must be developed to ensure an optimal functioning of the machine. In conclusion, it is impossible to reach 3000 W of heating capacity with the actual evaporator geometry. Other geometries will be studied to reach the 3000 limit of heating capacity.

7. CONCLUSION

The objective of this paper was to develop a semi-empirical model of an exhaust air heat pump. This model can predict the performance of the heat pump is the geometries of the constituting elements are changed. The results show a relative error on the electrical consumption of 13%, a maximum relative error on the condenser heat flow of 28 % and a relative error on the COP of 17%. The prediction of the condenser heat flow still have to be improved.

The results showed that the actual evaporator geometry limits the heating capacity of the machine and it is difficult to reach 3000 W of heating capacity, even with a compressor swept volume of 27 cm³. Other evaporators will be simulated to find the optimum geometry to reach the desired heating capacity, if possible.

Future research will deal with the new design of the machine and the test in laboratory. If necessary, different defrosting control strategies will be proposed and implemented.

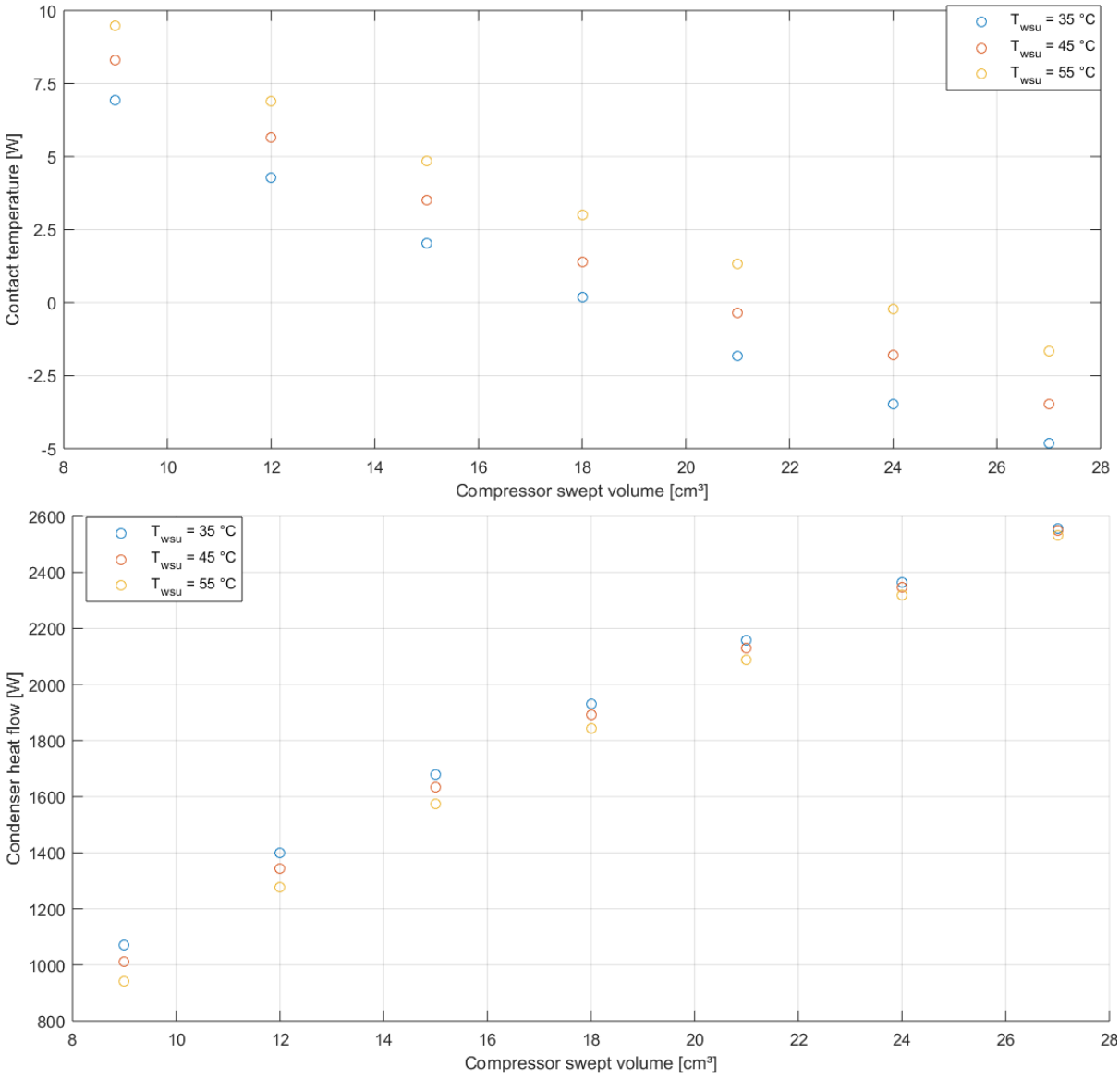

Figure 12: Influence of the compressor swept volume on the heat pump heating capacity

REFERENCES

Incropera, F.P., and DeWitt, D.P., 2002. *Fundamentals of Heat and Mass Transfer*. 5th ed. John Wiley & Sons, Hoboken, NJ.

Laverge, J., Janssens, A., 2012. *Heat recovery ventilation operation traded off against natural and simple exhaust ventilation in Europe by primary energy factor, carbon dioxide emission, household consumer price and exergy*. Energy and Buildings 50, pp 315–323.

Gendebien S., Georges E., Prieels L., Lemort V. 2013. *Experimental performance characterization of a new single room ventilation device with heat recovery*. Proceedings of the 34th AIVC conference.

Guyotab G., Shermanc M., Walkerc I. 2017. *Smart ventilation energy and indoor air quality performance in residential buildings: A review*. Energy and Buildings 165, pp 416-430.

Dechesne B., Gendebien S., Lemort V., Bertagnolio S. 2017. *Experimental investigation and dynamic modeling of an air-to-water residential heat pump with vapor injection and variable speed scroll compressor*. Proceedings of the 12th IEA Heat Pump Conference.

Nawaz K., Ahmed B., Elatar A., Baxter V., Abdelaziz O. 2017. *Performance optimization of CO2 heat pump water heater*. International Journal of Refrigeration, 85, pp 213-228.

Zhang J., Qin Y., Wang C. 2015. *Review on CO2 heat pump water heater for residential use in Japan.* Renewable and Sustainable Energy Reviews, 50, pp 1383-1391.

Underwood C.P. 2015. *Fuzzy multivariable control of domestic heat pumps.* Applied Thermal Engineering, 90, pp 957-969.

Fracastoro.V, Serraino.M. 2010. *Energy analyses of buildings equipped with exhaust air heat pumps (EAHP).* Energy and Buildings, 42 (8), pp 1283–1289.

Ransy F., Gendebien S., Lemort V. 2015. *Performances of a simple exhaust mechanical ventilation coupled to a mini heat pump: modeling and experimental investigations*. Proceedings of the 36th AIVC international conference.

Ransy F., Gendebien S., Lemort V. 2016. *Description of a Modelica-based thermal building model integrating multi-zone airflows calculation*. Proceedings of the 12th REHVA world congress CLIMA.

Ransy F., Sartor K., Gendebien S., Lemort V. 2018. *Performance analysis of a mini exhaust air heat pump integrated into a low energy detached house: experimental on-site performance.* Proceedings of the 5th International High Performance Building Conference.

Dardenne L., Fraccarib E., Maggioni A ., Molinaroli L., Proserpioc L., Winandy E. 2015. *Semi-empirical modelling of a variable speed scroll compressor with vapour injection.* International Journal of Refrigeration, 54, pp 76-87.

Giuffrida A. 2016. *A semi-empirical method for assessing the performance of an open-drive screw refrigeration compressor.* Applied Thermal Engineering, 93, pp 813-823.

Li W. 2013. *Simplified steady-state modeling for variable speed compressor.* Applied Thermal Engineering, 50, pp 318-326.

Winandy E., Saavedra C., Lebrun J. 2002. *Simplified modelling of an open-type reciprocating compressor.* International Journal of Thermal Sciences, 41, pp 183-192.

Lemort V., Quoilin S., Cuevas C., Lebrun J. 2009. *Testing and modeling a scroll expander integrated into an Organic Rankine Cycle.* Applied Thermal Engineering, 29, pp 3094-3102.

Martin H. 1996. *A theoretical approach to predict the performance of chevron-type plate heat exchangers.* Chemical Engineering and Processing, 35, pp 301-310.

Han, D., Lee, K., Kim, Y., 2003. *The characteristics of condensation in brazed plate heat exchangers with different chevron angles*. J. Korean Phys. Soc. 43 (1), 66–73.

Longo G., Righetti G., Zilio C. 2015. *A new computational procedure for refrigerant condensation inside herringbone-type Brazed Plate Heat Exchangers.* International Journal of Heat and Mass Transfer, 82, pp 530–536.

ASHRAE, 2000. *ASHRAE Handbook-HVAC Systems and Equipment*, Chapter 21. Atlanta: American Society of Heating, Refrigerating and Air-Conditioning Engineers, Inc.

Wang C., Chi K., Chang C. 2000. *Heat transfer and friction characteristics of plain fin-and-tube heat exchangers, part II: Correlation*. International Journal of Heat and Mass Transfer, 43, Issue 15, pp 2693-2700.

M.M. Shah. 1982. *Chart correlation for saturated boiling heat transfer: equations and further study*. ASHRAE Trans., Vol. 88, 185-196.